Received Jun.29 2020

Accepted Aug.3 2020

Article Type: Research Article

Edited by: Haiyun Ren, Beijing Normal University, China

Running Title: ABS6, SAV4, and KTN1 regulate cMT organization

ABNORMAL SHOOT 6 interacts with KATANIN 1 and SHADE AVOIDANCE 4 to promote cortical microtubule severing and ordering in *Arabidopsis*

Yuanfeng Li[1], Meng Deng[1], Haofeng Liu[1], Yan Li[1], Yu Chen[1], Min Jia[1,2], Hui Xue[1], Jingxia Shao[1], Jun Zhao[1], Yafei Qi[1], Lijun An[1], Fei Yu[1]*, Xiayan Liu[1]*

1.State Key Laboratory of Crop Stress Biology for Arid Areas and College of Life Sciences, Northwest A&F University, Yangling 712100, China

2. Present Address: Department of Plant & Microbial Biology, University of California Berkeley, CA 94720, United States of America

*Correspondences: Fei Yu (flyfeiyu@gmail.com); Xiayan Liu (xyliu@nwafu.edu.cn, Dr. Liu is fully responsible for the distribution of all materials associated with this article.)

Abstract

Plant interphase cortical microtubules (cMTs) mediate anisotropic cell expansion in response to environmental and developmental cues. In *Arabidopsis thaliana*,

KATANIN 1 (KTN1), the p60 catalytic subunit of the conserved MT-severing enzyme katanin, is essential for cMT ordering and anisotropic cell expansion. However, the regulation of KTN1-mediated cMT severing and ordering remains unclear. In this work, we report that the *Arabidopsis* IQ67 DOMAIN (IQD) family gene *ABNORMAL SHOOT 6* (*ABS6*) encodes a MT-associated protein. Overexpression of *ABS6* leads to elongated cotyledons, directional pavement cell expansion, and highly ordered transverse cMT arrays. Genetic suppressor analysis uncovered that ABS6-mediated cMT ordering is dependent on KTN1 and SHADE AVOIDANCE 4 (SAV4). Live imaging of cMT dynamics revealed that both ABS6 and SAV4 function as positive regulators of cMT severing. Furthermore, ABS6 directly interacts with KTN1 and SAV4 and promotes their recruitment to the cMTs. Finally, analysis of loss-of-function mutant combinations showed that ABS6, SAV4, and KTN1 work together to ensure the robust ethylene response in the apical hook of dark-grown seedlings. Together, our findings establish ABS6 and SAV4 as positive regulators of cMT severing and ordering, and highlight the role of cMT dynamics in fine-tuning differential growth in plants.

INTRODUCTION

Plant cell morphogenesis is under the complex regulation of developmental, hormonal, and environmental signals. Plant cytoskeletons play fundamental roles in cell morphogenesis, and the dynamic organization of interphase cortical microtubules (cMTs) underpins anisotropic cell expansion at the molecular level (Wasteneys 2000; Ehrhardt and Shaw 2006; Elliott and Shaw 2018). It is generally believed that transversely ordered cMT arrays are indicative of longitudinal cell elongation perpendicular to the cMT arrays (Lindeboom et al. 2013; Vineyard et al. 2013). However, the genetic factors that ensure the robust response of cMTs to internal and external cues remain elusive (Figure 1A).

cMT organization is modulated by diverse families of MT-associated proteins (MAPs) (Hamada 2014). One central group of MAPs is the MT-severing enzymes. Three meiotic clades of AAA ATPases, katanin, spastin, and fidgetin, catalyze the severing and disassembly of MTs (McNally and Roll-Mecak 2018). First isolated via biochemical approaches from a sea urchin egg extract, the widely conserved

katanin complex is composed of the p60 catalytic subunit and the p80 regulatory subunit (McNally and Vale 1993; Hartman et al. 1998). In *Caenorhabditis elegans*, the katanin p60 and p80 subunits were identified through the *meiosis defective 1* (*mei-1*) and *mei-2* mutants from a genetic screen for mutants with impaired meiosis (Srayko et al. 2000). In animal cells, katanin is responsible for severing MTs at spindle poles during cell division and is also important for organizing acentrosomal MT arrays (McNally and Thomas 1998; Roll-Mecak and Vale 2006). Given its critical roles, it is not surprising that katanin activities are tightly regulated. For example, the katanin-interacting protein abnormal spindle-like microcephaly associated (ASPM) works together with katanin to regulate spindle organization and neurodevelopment (Jiang et al. 2017). Recent systematic work has identified a large number of potential katanin binding proteins, presenting a complex picture of the katanin regulatory network (Cheung et al. 2016).

In *Arabidopsis thaliana*, the katanin p60 catalytic subunit, KATANIN 1 (KTN1), is encoded by a single copy gene, while the katanin p80 subunit is encoded by four homologous genes (Nakamura 2015; Wang et al. 2017). *Arabidopsis ktn1* mutants display disorganized cMT arrays, defective cell elongation, shortened hypocotyls, stunted growth, and were isolated in genetic screens for anisotropic cell expansion (the *botero1* alleles) (Bichet et al. 2001), interfascicular fiber development (the *fragile fiber 2* allele) (Burk et al. 2001), gibberellic acid (GA) response (the *GA5-LUC super expressor1* allele) (Bouquin et al. 2003), root morphogenesis (the *ectopic root hair 3* alleles) (Webb et al. 2002), and trichome branching (the *furca 2* alleles) (Luo and Oppenheimer 1999). The clustered regularly interspaced short palindromic repeats (CRISPR)/CRISPR-associated protein 9 (Cas9) gene-edited mutant *ktn80.1234*, in which all four p80 subunits are simultaneously mutated, resembles the *ktn1* mutant, supporting the conserved nature of the katanin complex (Wang et al. 2017). KTN1 has been extensively investigated for its function in cMT severing, ordering, and reorganization during mechanical stress response and blue light-induced phototropism in plants (Stoppin-Mellet et al. 2002; Wightman and Turner 2007; Nakamura et al. 2010; Uyttewaal et al. 2012; Lin et al. 2013; Lindeboom et al. 2013; Zhang et al. 2013; Sampathkumar et al. 2014; Nakamura 2015; Deinum et al. 2017). Both

experimental observation and mathematical modeling support that cMT severing by KTN1 at branching and crossover sites promotes the ordering of cMT arrays in plant cells (Wightman and Turner 2007; Zhang et al. 2013; Deinum et al. 2017).

Several regulators of KTN1 have also been identified in plants. In *Arabidopsis*, a Rho GTPase, Rho of Plants 6 (ROP6), acts through its effector protein ROP-interactive CRIB motif-containing protein 1 (RIC1) to promote cMT ordering (Fu et al. 2009). RIC1 directly binds to KTN1, activates its severing activities, and promotes cMT ordering (Lin et al. 2013). The *Arabidopsis* MAP SPIRAL2 (SPR2) modulates KTN1 activities (Wightman and Turner 2007; Wightman et al. 2013). It has been proposed that the localization of SPR2 to the cMT crossover sites prevents the severing of cMTs by KTN1, whereas the absence of SPR2 increases cMT severing frequency and ordering (Wightman et al. 2013). In addition, augmin complexes could localize to the cMT crossover sites and suppress KTN1-mediated cMT severing and ordering (Wang et al. 2018; Tian and Kong 2019). Despite these findings, how katanin activity is regulated in plants is only beginning to be revealed.

In this work, aiming at identifying regulators of anisotropic cell expansion, we identified a gain-of-function *Arabidopsis* mutant *abnormal shoot 6-1D* (*abs6-1D*, D for dominant) displaying elongated cotyledons, altered pavement cell morphology, and highly ordered transverse cMT arrays. We showed that *ABS6* encodes an IQ67 DOMAIN (IQD) family MAP. Extensive genetic suppressor screen revealed that ABS6-mediated elongated growth and cMT ordering require KTN1 and SHADE AVOIDANCE 4 (SAV4). Furthermore, we established that both ABS6 and SAV4 act as positive regulators of cMT severing. ABS6 directly interacts with KTN1 and SAV4 and promotes their localization to the cMTs. In addition, analysis of loss-of-function mutant combinations revealed that the collective activities of ABS6, SAV4, and KTN1 are necessary for the robust response of apical hook to plant hormone ethylene in dark-grown seedlings. These findings demonstrate that ABS6 interacts with KTN1 and SAV4 to promote cMT severing and ordering in *Arabidopsis*.

RESULTS

ABS6 promotes anisotropic cell expansion and cMT ordering

To uncover the genetic factors controlling anisotropic cell expansion, we used the cotyledon shape of *Arabidopsis* seedlings as a readout of aberrant cell elongation, and identified a semi-dominant, gain-of-function mutant, *abs6-1D*, from our activation tagging mutant population (Jia et al. 2019). The most striking phenotype of the *abs6-1D* mutant was its long and narrow cotyledons, in stark contrast to the round cotyledons of the wild type (WT) (Figures 1B, S1A). The combination of the increased cotyledon length and the reduced cotyledon width resulted in a dramatic increase of the cotyledon leaf index (leaf length/leaf width) in the *abs6-1D* mutant (Figure S1B). Elongated growth was also observed in other organs of the *abs6-1D* mutant, including rosette leaves, siliques, and seeds (Figure S1C–G). However, hypocotyl elongation in etiolated seedlings was not affected in the *abs6-1D* mutant (Figure S1H, I).

We focused on cotyledons for further analysis because of the prominent elongated growth of this organ in the *abs6-1D* mutant. At the cellular level, epidermal pavement cells (PCs) in WT cotyledons had a typical interlocked "jigsaw-puzzle" arrangement, while in *abs6-1D* cotyledons PCs were nearly rectangular with less prominent indentations and lobes (Figure 1B). In addition, most PCs in the *abs6-1D* mutant expanded along the proximo-distal axis, while there was no consistent direction for WT PC expansion (Figure 1B). To determine whether the directional PC expansion in the *abs6-1D* mutant was caused by an alteration in cMT arrays, we probed cMT patterns in WT and *abs6-1D* seedlings using a green fluorescent protein (GFP)-BETA-6 TUBULIN (TUB6) fusion protein (GFP-TUB6) as a MT marker (Nakamura et al. 2004). Consistent with the anisotropic expansion of PCs, cMTs formed highly ordered transverse arrays that were perpendicular to the direction of cell elongation in *abs6-1D* PCs, in contrast to the randomly oriented cMTs in WT PCs (Figure 1B). Quantification of cMT angles confirmed that the proportion of transverse cMTs (−10° to 10°) was highly elevated in *abs6-1D* PCs (Figure 1C).

To reveal the genetic lesion in the *abs6-1D* mutant, we determined that the activation tagging T-DNA was inserted between *At4g10630* and *At4g10640*, with the CaMV 35S enhancer sequences facing *At4g10640* (Figure S2A). Reverse transcription quantitative PCR (RT-qPCR) analyses showed that *At4g10640* was upregulated in the *abs6-1D* mutant (Figure S2B). More importantly, transgenic lines over-expressing a 35S promoter-driven *At4g10640-GFP* fusion gene in the WT background resembled the *abs6-1D* mutant at the organismal, tissue, and cellular levels (Figure S2C–G), strongly suggesting that activation of *At4g10640* expression is the cause for the elongated growth phenotype of the *abs6-1D* mutant. Therefore, we named *At4g10640 ABNORMAL SHOOT 6* (*ABS6*). Histochemical β-glucuronidase (GUS) staining of the *pABS6:GUS* line showed that *ABS6* is expressed in light- and dark-grown seedlings (Figure S2H). RT-qPCR analysis with RNAs extracted from different plant tissues confirmed the presence of *ABS6* transcripts in all tissues examined, with relatively higher expressions in young shoots, roots, flowers, and siliques, suggesting an active role for ABS6 in different plant tissues (Figure S2I). Together, our findings support a critical role for ABS6 in promoting cMT ordering, directional cell expansion, and elongated growth.

The C-terminal half of ABS6 binds and bundles MTs

ABS6/*At4g10640* encodes IQ67 DOMAIN 16 (IQD16), a member of the plant-specific IQD protein family (Abel et al. 2005). Recent studies have implicated some IQD proteins as plant MAPs (Bürstenbinder et al. 2013; Bürstenbinder et al. 2017; Sugiyama et al. 2017; Liang et al. 2018). To investigate whether ABS6/IQD16 is a *bona fide* MAP, we first crossed the *p35S:ABS6-GFP* line into the *monomeric red fluorescent protein* (*mRFP*)-*TUB6* background (Ambrose et al. 2011). We observed that ABS6-GFP decorated cMTs in cotyledon PCs (Figure 1D, E). Expressing endogenous promoter-driven *ABS6-GFP* (*pABS6:ABS6-GFP*) in mesophyll protoplasts from the *mRFP-TUB6* line also showed overlapping ABS6-GFP and mRFP-TUB6 signals (Figure S2J). To identify the MT binding region of ABS6, full-length ABS6 (1–423 aa) and two truncated versions of ABS6, ABS6_N (1–200 aa) containing the IQ motifs and ABS6_C (201–423 aa) (Figure 1F), were fused with GFP and transiently expressed in mesophyll protoplasts from

the *mRFP-TUB6* line. ABS6-GFP and ABS6_C-GFP showed filamentous signals that overlapped with cMTs, while ABS6_N-GFP showed punctate signals that were generally not associated with cMTs (Figure 1G). To further verify that ABS6 could directly bind to MTs via its C-terminal half, we carried out the *in vitro* co-sedimentation assay using a recombinant ABS6_C with both a N-terminal maltose binding protein (MBP) tag and a C-terminal 6×His tag (designated M-ABS6_C-H). In the absence of MTs, M-ABS6_C-H was mostly present in the supernatant after ultracentrifugation (Figure 1H). However, when M-ABS6_C-H was incubated with MTs, ultracentrifugation led to co-sedimentation of M-ABS6_C-H with MTs (Figure 1H), suggesting a direct interaction between ABS6_C and MTs.

Unexpectedly, when compared with protoplasts expressing full-length ABS6-GFP, protoplasts expressing ABS6_C-GFP not only had brighter mRFP-TUB6 signals but also had cMTs that were more resistant to the MT depolymerization drug oryzalin, suggesting a possible MT bundling effect of ABS6_C (Figures 1G, 2A). Consistent with this effect, an *in vitro* tubulin polymerization assay indicated that M-ABS6_C-H enhanced tubulin polymerization to a greater extent than taxol, a drug known to stabilize MTs (Figure 2B). Furthermore, incubating M-ABS6_C-H with MTs *in vitro* induced MT bundles that were sensitive to 0.2 M NaCl (Figure 2C). Together, these data support that ABS6/IQD16 is a MAP and the C-terminal half of ABS6/IQD16 binds and bundles MTs.

ABS6-mediated cMT ordering requires KTN1 and SAV4

To gain mechanistic insight into how ABS6 promotes cMT ordering and identify additional genetic factors regulating cMT ordering, we performed ethyl methanesulfonate (EMS) mutagenesis in the *abs6-1D* mutant and screened for suppressor mutants that could reverse the elongated cotyledon phenotype. Eight suppressor mutants were identified and placed into two complementation groups. *ABS6* expression levels in the suppressor lines were similar to that in the *abs6-1D* mutant, confirming that the suppression of *abs6-1D* phenotype was not due to the silencing of *ABS6* expression (Figure S3A). The first group consisted of seven

recessive suppressors that phenotypically resembled mutants of the *Arabidopsis KTN1* gene, which encodes the lone p60 catalytic subunit of the MT-severing enzyme katanin (Bichet et al. 2001; Burk et al. 2001; Webb et al. 2002; Bouquin et al. 2003). Point mutations were identified in the *KTN1* locus in each of these mutants; thus, these new alleles were named *ktn1-7* to *ktn1-13*, and *ktn1-7* was used for further analyses (Figures 3A, S3B–D). Functional complementation with the endogenous promoter-driven *GFP-KTN1* (*pKTN1:GFP-KTN1*) in the *ktn1-7 abs6-1D* background reversed the suppressor to the *abs6-1D* phenotype, and restored the WT phenotype in the *ktn1-7* background (Figure S3E-H). These data establish that ABS6-mediated directional elongated growth is dependent on KTN1.

The second complementation group included one recessive mutant. A map-based cloning procedure identified a point mutation converting the Gln^{378} codon to a stop codon in *At5g10200* in the suppressor line (Figures 3B, S4A). *At5g10200* was reported as *SHADE AVOIDANCE 4* (*SAV4*), encoding a plant-specific protein harboring two N-terminal armadillo (ARM) domains and a C-terminal tetratricopeptide (TPR) domain (Figure 3B; Ge et al. 2017). We therefore named our allele *sav4-2*. Expression of endogenous promoter-driven *SAV4-GFP* (*pSAV4:SAV4-GFP*) in the *sav4-2 abs6-1D* background restored the *abs6-1D*-like elongated growth, confirming that the lack of *SAV4* caused the suppression of the *abs6-1D* phenotype (Figure S4B, D). The *sav4-2* single mutant displayed modest cell elongation defects including shortened petioles, which could also be complemented by expressing *pSAV4:SAV4-GFP* (Figure S4C, E).

At the organismal level, the *ktn1-7 abs6-1D* mutant showed slightly ovate cotyledons that were greatly reduced in length compared to the *abs6-1D* mutant, indicating that the *ktn1-7* mutation strongly suppressed the *abs6-1D* phenotype (Figure 3C, D). The *sav4-2* mutation was a weaker suppressor and the *sav4-2 abs6-1D* mutant showed elliptic cotyledons (Figure 3C, D). At the cellular level, the excessive PC elongation in the *abs6-1D* mutant was alleviated by the presence of either the *ktn1-7* or *sav4-2* mutant alleles (Figure 3C, E). However, PCs in *ktn1-7 abs6-1D* or *sav4-2 abs6-1D* double mutants still showed more directional cell expansion than in the *ktn1-7* or *sav4-2* single mutants, suggesting that the effect of

increased expression of *ABS6* on directional cell expansion is not entirely dependent on KTN1 or SAV4 (Figure 3C). Importantly, the highly ordered transverse cMT arrays in *abs6-1D* PCs were abolished by the presence of the *ktn1-7* or *sav4-2* alleles, establishing a role of MTs in the suppression of the *abs6-1D* phenotype (Figure 3C, F). Together, our genetic data establish that KTN1 and SAV4 are required for ABS6-mediated cMT ordering.

ABS6 and SAV4 are positive regulators of cMT severing

Given the central role of cMT severing in organizing and ordering cMT arrays, we quantified cMT severing events in cotyledon PCs of the WT, the *abs6-1D* mutant, and *abs6-1D* suppressor lines with time-lapse confocal imaging. In line with previous reports, a median severing frequency of 18 (interquartile range, IQR 15–22) $\times 10^{-3}$ events/μm^2/min was observed in the WT (Figure 4A; Fan et al. 2018). In the *abs6-1D* mutant, an astonishing ~50% increase in the severing frequency (median 28, IQR 21–32 $\times 10^{-3}$ events/μm^2/min) was observed (Figure 4A). In the absence of a functional KTN1, severing of cMTs was abolished with or without the *abs6-1D* mutation (Figure 4A), indicating that KTN1 activities are indispensable for cMT severing. This finding is in agreement with previous reports that KTN1 is solely responsible for cMT severing in *Arabidopsis* PCs (Nakamura et al. 2010; Zhang et al. 2013).

Notably, the severing frequency was also lower in the *sav4-2 abs6-1D* double mutant (median 20, IQR 14.5–20 $\times 10^{-3}$ events/μm^2/min) than in the *abs6-1D* mutant (Figure 4A), providing an explanation for the suppression of elongated organs in the *sav4-2 abs6-1D* double mutant. Consistent with this finding, the *sav4-2* single mutant showed a significantly reduced cMT severing frequency (median 12, IQR 10–15.75 $\times 10^{-3}$ events/μm^2/min) compared to that of the WT (Figure 4A), establishing SAV4 as a previously unrecognized positive regulator of cMT severing. The extent of the reduction in severing frequencies caused by the *ktn1-7* or *sav4-2* mutations correlated with the degree of inhibition of elongated growth in their respective suppressor lines (Figure 4A).

We examined how ABS6 and SAV4 promote cMT severing by quantifying two parameters: "severing waiting time" (defined as the time elapsed since the formation of the MT crossover until the completion of MT severing) and "severing probability" (defined as the percentage of newly formed crossovers that were severed during the observation period) in WT, *asb6-1D*, and *sav4-2* PCs. The "severing waiting time" was comparable in all three genotypes, i.e. the time required for severing to occur was unchanged in the *abs6-1D* or the *sav4-2* mutant compared with that in the WT (Figure 4B). By contrast, the severing probability was significantly higher in the *abs6-1D* mutant but lower in the *sav4-2* mutant compared to the WT (Figure 4C). These observations suggest that ABS6 and SAV4 promote severing by enabling more crossover sites to become severing substrates. To further explore this hypothesis, we investigated whether ABS6 and SAV4 modulate the localization of GFP-KTN1. We compared GFP-KTN1 localizations in WT, *abs6-1D*, and *sav4-2* backgrounds. Indeed, the proportion of cMT crossovers coinciding with GFP-KTN1 foci increased considerably in the *abs6-1D* mutant, but decreased in the *sav4-2* mutant compared with that in the WT, suggesting that both ABS6 and SAV4 act as positive regulators for the localization of GFP-KTN1 to cMT crossover sites (Figure 4D, E). Together, these results suggest that ABS6 and SAV4 promote cMT severing by enhancing the recruitment of the severing enzyme KTN1 to cMT crossovers.

ABS6 directly interacts with KTN1

We tested whether ABS6 promotes cMT ordering and severing through a direct interaction with KTN1. In a yeast two-hybrid assay, the C-terminal half of ABS6 (ABS6_C), but not full-length ABS6, interacted with KTN1 (Figure 5A). MBP-tagged ABS6_C can be co-immunoprecipitated with His-tagged KTN1 by a KTN1 antibody *in vitro* (Figure 5B). In bimolecular fluorescence complementation (BiFC) assays, yellow fluorescent protein (YFP) fluorescence was observed when ABS6_C fused with the N-terminal half of YFP (YN-ABS6_C) was co-expressed with KTN1 fused with the C-terminal half of YFP (KTN1-YC) in protoplasts and the YFP signals generated by the interaction of YN-ABS6_C and KTN1-YC overlapped with mRFP-TUB6-labeled cMTs (Figures 5C, S5A). However,

co-expressing YN-ABS6 with KTN1-YC did not yield YFP signals. We noted that when YN alone was co-expressed with KTN1-YC, filamentous cMTs were scarce, while when YN-ABS6_C was expressed either with YC or KTN1-YC, cMTs were stabilized in protoplasts, probably due to the MT bundling effect of ABS6_C (Figures 5C, S5A). Based on these observations, we reasoned that detection of the interaction of full-length ABS6-KTN1 in the BiFC assay may be hindered by cMT destabilization due to the overexpression of active KTN1.

To capture the ABS6-KTN1 interaction, we introduced a R402A mutation in KTN1. Arg402 corresponds to Arg351 in the *C. elegans* katanin p60 subunit, which is indispensable for its ATPase and severing activity (Figure S5B) (Zehr et al. 2017). Indeed, when GFP-KTN1^{R402A} was expressed in protoplasts from the *mRFP-TUB6* line in the *ktn1-7* background, in which endogenous KTN1 was also absent, cMTs were preserved, in contrast to the rare presence of short cMT pieces in *mRFP-TUB6* protoplasts expressing GFP-KTN1 (Figure S5C). Co-expressing YN-ABS6 and KTN1^{R402A}-YC in *ktn1-7 mRFP-TUB6* protoplasts generated YFP signals decorating cMTs (Figures 5D, S5D). Finally, we performed immunoprecipitation with membrane fractions of *p35S:ABS6-GFP* transgenic lines, since cMTs are associated with the plasma membrane in plants (Dixit and Cyr, 2004). Using GFP-Trap beads, KTN1 was co-immunoprecipitated with ABS6-GFP, providing validation for the interaction between full-length ABS6 and KTN1 *in planta* (Figure 5E). Together these data establish ABS6 as an interacting partner of the key MT-severing enzyme KTN1.

ABS6 interacts with SAV4 via its C-terminal half

The suppression of the *abs6-1D* phenotype by the loss of *SAV4* and the unexpected finding of SAV4 as a positive regulator of cMT severing prompted us to test whether ABS6 also interacts with SAV4. In a yeast two-hybrid assay, although we did not detect an interaction between SAV4 and full-length ABS6, SAV4 showed unambiguous interaction with the C-terminal half of ABS6, ABS6_C (Figure 6A). In addition, a recombinant GST-SAV4 fusion protein was able to pull down recombinant M-ABS6_C-H *in vitro* (Figure 6B), confirming that the C-terminal half of ABS6 could bind SAV4. Next, we evaluated the interaction

between ABS6_C and SAV4 in protoplast-based BiFC assays. Co-expression of YN-SAV4 and ABS6_C-YC in protoplasts of *mRFP-TUB6* lines not only reconstituted YFP signals but also lead to destabilization of cMTs (Figures 6C, S5E). In 57.1% of the cells observed, cMTs were scarce and short but still recognizable and the YFP signals overlapped with cMTs (Figure 6C). In 42.9% of the cells observed, YFP signals appeared as discrete foci at the cell cortex while filamentous cMTs were absent (Figure 6C).

To explore the consequence of the probable ABS6-SAV4 interaction *in vivo*, we first examined the subcellular localization of SAV4-GFP with z-stack confocal imaging in *pSAV4:SAV4-GFP* transgenic lines. Consistent with a previous report, in the root meristem zone, SAV4-GFP was observed in the nucleus and on the plasma membrane (Figure S6A; Ge et al. 2017). In the root elongation and maturation zone, nuclear SAV4-GFP signals decreased and SAV4-GFP signals were mostly present on the plasma membrane and at the cell cortex as punctate dots (Figure S6B, C). In the hypocotyl, SAV4-GFP signals were observed in the nucleus, on the plasma membrane, and at the cell cortex (Figure S6D). To explore whether SAV4-GFP puncta could localize to cMTs, we crossed the *pSAV4:SAV4-GFP* line into the *p35S:mRFP-TUB6* MT marker line and examined SAV4-GFP puncta and cMTs in cotyledon PCs. Similar to the observations with other tissues, SAV4-GFP signals were on the plasma membrane and as punctate dots at the cell cortex in PCs of the *SAV4-GFP mRFP-TUB6* dual-labeled lines. Some cortical SAV4-GFP puncta were observed on cMTs (Figure S6E).

We further crossed the *pSAV4:SAV4-GFP p35S:mRFP-TUB6* dual-labeled line into the *abs6-1D* background and compared MT localization of SAV4-GFP in WT and a*bs6-1D* backgrounds. Quantification of the proportion of SAV4-GFP puncta residing on cMTs revealed that more SAV4-GFP puncta were present on cMTs in the *abs6-1D* background than in the WT background (Figure 6D, E). These findings suggest that ABS6 interacts with SAV4 and promotes the recruitment of SAV4 to cMTs *in planta*.

ABS6, SAV4, and KTN1 contribute to the robust ethylene response in the apical hook

The activation of *ABS6* leads to elongated organ growth and increased cMT ordering; however, the phenotypes of both light- and dark-grown seedlings of *ABS6* loss-of-function mutants (*abs6-1*/*SALK_053223* and *abs6-2*/*SAIL_560_E08*) were indistinguishable from that of the WT (Figure S7A-E). We also did not observe differences in the severing frequency in cotyledon PCs of WT and *abs6-1* seedlings (Figure S7F). These results suggest that ABS6 is dispensable for normal growth. Given the MT severing-promoting function of ABS6, we reasoned that developmental processes that demand rapid cMT reorganization may be more dependent on ABS6.

The plant hormone ethylene induces fast reorientation of cMT arrays in hypocotyl epidermal cells of etiolated seedlings (Ma et al. 2016). At the organismal level, ethylene-mediated differential growth leads to the exaggeration of the apical hook, a hallmark of the ethylene triple response (Guzman and Ecker 1990). Interestingly, treatment with either the MT-destabilizer oryzalin or the MT-stabilizer taxol reduced the hook angles of etiolated seedlings and abolished the hook exaggeration caused by the *constitutive triple response1-1* (*ctr1-1*) mutation or treatment with the ethylene precursor 1-aminocyclopropane-1-carboxylic acid (ACC) (Figure 7A, B; Kieber et al. 1993). These observations suggest that functional cMTs are required for the differential growth in the apical hook region and prompted us to test whether ABS6, SAV4, and KTN1 are involved in this process.

Next, we analyzed apical hook bending phenotypes in dark-grown WT seedlings and mutants of *ABS6*, *SAV4*, and *KTN1* under mock or ACC treatment (Figure 7C, D). WT seedlings showed a median hook angle of 183.8º under the mock treatment and 252.6º under ACC treatment (Figure 7C, D). The loss of *ABS6* alone did not affect hook formation or hook exaggeration in response to ACC (Figure 7C, D). The *sav4-2* mutant showed reduced apical hook tightening (median hook angle: 175.0º) and hook exaggeration under ACC treatment (median hook angle: 197.4º) compared with the WT (Figure 7C, D), suggesting that SAV4 plays a

role in the differential growth during hook formation. In the *abs6-1 sav4-2* double mutant, the extent of hook tightening was similar to that of the *sav4-2* single mutant under mock treatment (Figure 7C, D). However, under ACC treatment, the median hook angle in the *abs6-1 sav4-2* double mutant was 167.9º, which was significantly lower than that in the *sav4-2* mutant, indicating that the *abs6-1* mutation exacerbated the hook formation defects of the *sav4-2* mutant in response to ethylene (Figure 7C, D). In addition, hook angles were highly variable in the *abs6-1 sav4-2* double mutant, displaying a much wider distribution skewed toward smaller values compared with that of the *sav4-2* mutant (*sav4-2*: IQR 177.2–220.2º; *abs6-1 sav4-2*: IQR 102.3–197.8º; Figure 7C, D). To confirm the role of *ABS6* in ethylene-induced hook exaggeration, we performed the same analyses with the *abs6-2* mutation, a second loss-of-function allele of *ABS6*, and obtained similar results (Figure S8).

Consistent with the essential role of KTN1 in cMT organization, hook angle abnormalities were more pronounced in mutants lacking a functional KTN1 (Figure 7C, D). Without ACC, the *ktn1-7* mutant showed a greatly reduced hook angle (median hook angle: 73.15º) compared to that of the WT (Figure 7C, D), suggesting that KTN1 is critical for the differential growth of the apical hook in the dark. Although much reduced, *ktn1-7* seedlings still showed a small but significant response to ACC in the apical hook (median hook angle: 108.3º Figure 7C, D). The addition of the *abs6-1* mutation also further reduced the hook angle in mock- or ACC-treated *abs6-1 ktn1-7* seedlings (mock: 55.3º; ACC: 85.9º) compared with the *ktn1-7* single mutant (Figure 7C, D). Together, our data suggest that ABS6, SAV4, and KTN1 work together to ensure the robust response of the apical hook to ethylene in dark-grown seedlings.

DISCUSSION

The MT cytoskeleton plays essential functions in cell division, expansion, and morphogenesis. In plants, interphase cMTs regulate differential cell growth through the guidance of cell wall biosynthesis (Baskin 2001; Paredez et al. 2006; Gutierrez et al. 2009). In response to developmental signals and environmental cues, cMTs undergo dynamic rearrangements, often facilitated by the actions of MAPs (Chen et

al. 2016). However, the molecular mechanism underlying cMT-mediated differential cell growth remains elusive. We are interested in identifying regulators of anisotropic cell expansion (Wang et al. 2015). Through large-scale genetic screening of an activation tagging mutant population in the model plant *Arabidopsis*, we identified a gain-of-function mutant, *abs6-1D*, displaying excessive elongated growth of cotyledons, leaves, and floral organs. We show here that ABS6 is a plant-specific IQD protein and a MAP, which directly binds to MTs via its C-terminal half (Figure 1). The signature of IQD family proteins is the presence of repetitive IQ motifs, which confer putative calmodulin-binding capacities (Abel et al. 2005). The founding member of the *IQD* gene family is the *SUN* locus in tomato (*Solanum lycopersicum*) (Xiao et al. 2008). As the major quantitative trait locus (QTL) for tomato fruit shape, the underlying cause for the elongated fruit shape determined by the *SUN* locus is the activated expression of *IQD12* due to a retrotransposon-mediated gene duplication (Xiao et al. 2008). An increasing body of evidence suggests that IQD family proteins are important regulators of cell and plant morphogenesis, and some IQD proteins are MAPs (Bürstenbinder et al. 2013; Bürstenbinder et al. 2017; Sugiyama et al. 2017; Liang et al. 2018). In the *abs6-1D* mutant, we show that the activated *ABS6* expression causes an increase in the cMT severing frequency and ordering of transverse cMT arrays in PCs (Figures 1, 4), providing an explanation for the elongated growth phenotype.

The elongated growth of *abs6-1D*, as well as the underlying molecular cMT signature, provides a unique platform to identify regulators of cMT organization and cell morphogenesis. Through in-depth genetic screening for *abs6-1D* suppressors, we discovered that KTN1 and SAV4 are required for ABS6-mediated cMT ordering (Figure 3). KTN1 is known as the key regulator of cMT ordering through its MT-severing activity, confirming the rationale of our genetic screen (Lin et al. 2013; Zhang et al. 2013; Deinum et al. 2017). SAV4 was previously reported to participate in the shade avoidance response, potentially through its involvement in regulating auxin homeostasis (Ge et al. 2017). Unexpectedly, we established SAV4 as a previously unknown positive regulator of cMT severing (Figure 4). Time-lapse confocal imaging revealed that the probability of severing at

cMT crossover sites was increased in the *abs6-1D* mutant but reduced in the *sav4-2* mutant (Figure 4C). Consistent with this notion, quantitative analysis of GFP-KTN1 localization showed that the recruitment of KTN1 to cMT crossover sites was positively regulated by ABS6 and SAV4 (Figure 4D, E). Moreover, functional connections between ABS6, KTN1 and SAV4 were underpinned by their physical interactions (Figures 5, 6). Interestingly, for both SAV4 and KTN1, we detected their interaction only with the C-terminal half of ABS6 in yeast two-hybrid and BiFC assays, suggesting that the interaction between the full-length ABS6 and KTN1 or SAV4 may be too transient to capture or requires additional proteins to adjust the conformation of ABS6 for interaction. Nonetheless, our findings uncovered new mechanisms for the regulation of KTN1-mediated cMT severing in plants.

Finally, we placed the genetic and physical interactions of ABS6-KTN1 and ABS6-SAV4 into the physiological context of ethylene responses in the apical hook. We discovered that the ethylene-induced exaggeration of the apical hook requires functional cMTs and the collective activities of ABS6, SAV4, and KTN1 (Figure 7). SAV4 and KTN1 are required for proper hook formation and its response to ethylene treatment. Although we did not find a conspicuous phenotype in the single loss-of-function mutant of *ABS6*, we did find that the *abs6-1 sav4-2* double mutant displayed a less robust response to ethylene in the apical hook compared with the *sav4-2* single mutant (Figure 7C, D). The inclusion of the *abs6-1* mutation also further attenuated the responsiveness of the *ktn1-7* mutant to ethylene in the *abs6-1 ktn1-7* double mutant (Figure 7C, D). The relatively subtle effect of ABS6 on apical hook formation suggests that sessile higher plants may have evolved factors to fine-tune the robustness of cMT responses to developmental or environmental signals (Mestek Boukhibar and Barkoulas 2016). A similar case is seen in the plant-specific TON1 Recruiting Motif (TRM) family of MAPs, which regulate the orientation of the cell division plane in a subtle way (Schaefer et al. 2017).

Taken together, our data identified two previously unknown plant-specific positive regulators of cMT severing and ordering, ABS6 and SAV4. Along with the

canonical MT-severing enzyme KTN1, these three proteins interact and modulate cMT severing and ordering, thus enabling anisotropic cell elongation (Figure 7E). Furthermore, cMT organization controlled by the coordinated action of ABS6, SAV4, and KTN1 provides a MT-based mechanism at the molecular level for the ethylene-induced apical hook exaggeration at the organismal level in *Arabidopsis*.

MATERIALS AND METHODS

Plant growth conditions

Arabidopsis thaliana seeds were stratified at 4°C for 2 days and grown on Jiffy-7-Peat Pellets (Jiffy Group) or on commercial soil mix (Pindstrup), under continuous illumination of ~100 μmol m^{-2} s^{-1} at 22°C. For protoplast preparation, plants were maintained on a 12 h/12 h day/night cycle at 22°C. For seedling analyses, seeds were surface sterilized and grown on 1/2 Murashige and Skoog (MS) medium (M153, PhytoTechnology Laboratories) supplemented with 1% Bacto agar (214010, BD) and 1% sucrose under continuous illumination of ~100 μmol m^{-2} s^{-1} at 22°C.

Plant materials

WT refers to the *Arabidopsis* ecotype Columbia-0 (Col-0) in this study. All the *Arabidopsis* strains used in this study are in the Col-0 background except the Landsberg *erecta* (L*er*) ecotype used for molecular mapping. The MT marker lines *p35S:GFP-TUB6* (CS6550) and *p35S:mRFP-TUB6* (CS67066) have been described and were obtained from the *Arabidopsis* Biological Resource Centre (ABRC) (Nakamura et al. 2004; Ambrose et al. 2011). The *ctr1-1* mutant has been described (Kieber et al. 1993). The T-DNA insertion lines *abs6-1* (*SALK_053223*) and *abs6-2* (*SAIL_560_E08*) were obtained from the ABRC. The *abs6-1D* mutant, the new *ktn1* alleles *ktn1-7* to *ktn1-13*, and the *sav4-2* mutant were identified in this study. The double mutants *abs6-1 ktn1-7*, *abs6-1 sav4-2*, and *abs6-2 sav4-2* were generated in this study. The *p35S:ABS6-GFP*, *pKTN1:GFP-KTN1*, and *pSAV4:SAV4-GFP* transgenic lines were produced by the *Agrobacterium tumefaciens*-mediated floral dip plant transformation method (Clough and Bent

1998). Homozygous fluorescent lines were crossed into various genetic backgrounds as needed. See Table S1 for a summary of *Arabidopsis* strains used in this study.

Spinning-disk confocal microscopy imaging

Imaging experiments were performed with a spinning-disk confocal system built on a DMi8 inverted microscope (Leica) equipped with a CSU-W1 confocal scanner unit (Yokogawa) and an iXon Ultra 888 EMCCD camera (Andor). GFP and YFP were excited at 488 nm. mRFP, mCherry, and propidium iodide (PI) fluorescent dye were excited at 561 nm. Images were acquired using the IQ3.0 Imaging Workstation software (Andor).

Imaging of cMTs in Figures 1B, 3C, and S2C, and time-lapse imaging of cMT severing activities were performed with a HC PL APO 63× N.A.1.30 glycerol objective (Leica). Dual imaging of ABS6-GFP/GFP-KTN1/SAV4-GFP and mRFP-TUB6 in transgenic lines and imaging of protoplasts were performed with a HCX PL Apo 1.44 N.A. 100× oil immersion objective. Imaging of cell outlines was performed with a HC PL APO 20× N.A. 0.80 objective or a HC PL APO 40× N.A. 0.85 objective. Z-stack imaging of SAV4-GFP was performed with a 0.5 µm z-step using a HC PL APO 63× N.A.1.30 glycerol objective (Leica).

Since cMTs are tightly associated with the plasma membrane, when focusing to the central layer of the cell, GFP-TUB6 shows the outline of the cell. Thus, GFP-TUB6 was used for imaging the outlines of cotyledon abaxial PCs shown in Figures 1B, 3C, and S7C. For *p35S:ABS6-GFP* lines, the outlines of cotyledon abaxial PCs were stained by PI (1 mg ml^{-1} in H_2O).

Quantitative analysis of confocal images

To quantify cMT angles in various genetic backgrounds, the angles of individual cMTs were measured with Fiji-ImageJ. cMTs that were perpendicular to the cotyledon proximo-distal axis were considered as 0°.

GFP-TUB6-labeled cMTs were captured by time-lapse confocal imaging with a 300 ms exposure time at 2–3 s intervals for at least 5 min. For each cell, a 10 μm × 10 μm ROI was selected for manually scoring severing events over 5 min. Severing events were determined as described (Zhang et al. 2013; Fan et al. 2018). To determine the severing frequency, both severing events at pre-existing crossovers and at newly formed crossovers (either formed by an encounter of two MTs or formed by a nucleation event) were counted during the 5-min imaging period. Severing frequencies in Figure 4A were determined from: WT, n = 197 events in 21 ROIs; *abs6-1D*, n = 289 events in 21 ROIs; *ktn1-7 abs6-1D*, n = 0 events in 20 ROIs; *sav4-2 abs6-1D*, n = 181 events in 20 ROIs; *ktn1-7*, n = 0 events in 20 ROIs; *sav4-2*, n = 125 events in 20 ROIs. Severing frequencies in Figure S7F were determined from: WT, n = 198 events in 21 ROIs; *abs6-1*, n = 182 events in 20 ROIs.

Severing events at newly formed crossovers were used to determine the severing waiting time and severing probability. The severing waiting time was defined as the time elapsed since the frame when the crossover was formed until the frame when a cMT severing event was completed. Severing waiting time was determined from: WT, n = 61 events in 17 ROIs; *abs6-1D*, n = 97 events in 23 ROIs; *sav4-2*, n = 55 events in 20 ROIs. To determine the severing probability, the number of newly formed crossovers during the 5-min imaging period (i.e. number of newly formed crossovers) were scored with the Pointpicker plug-in in Fiji-ImageJ. Total numbers of newly formed crossover events scored were as follows: WT, n = 2467 in 21 ROIs; *abs6-1D*, n = 2071 in 21 ROIs; *sav4-2*, n = 2245 in 20 ROIs. Severing probability was calculated as the number of severing events at the newly formed crossovers divided by the number of newly formed crossovers for each ROI.

To quantify GFP-KTN1 localization in WT, *abs6-1D*, and *sav4-2* cells, the number of crossovers in 10 randomly selected ROIs were scored with the Pointpicker plug-in in Fiji-ImageJ for each genotype. The proportion of cMT crossovers with GFP-KTN1 puncta was calculated for each ROI. To quantify SAV4-GFP localization in WT and *abs6-1D* cells, the number of SAV4-GFP

puncta in 20 randomly selected ROIs were scored with the Pointpicker plug-in in Fiji-ImageJ for each genotype. The proportion of MT-localized SAV4-GFP puncta was calculated for each ROI.

In vitro co-immunoprecipitation (Co-IP) and pull-down assays

For the *in vitro* Co-IP assay, 10 μg of His-KTN1 was first incubated with 20 μl of anti-KTN1 antibody-conjugated Protein A Sepharose beads (17-1279-01, GE Healthcare) in 1 ml IP buffer (20 mM HEPES pH 7.5, 100 mM NaCl, 3 mM $MgCl_2$, 1 mM DTT, 0.1% Triton X-100, and 1 mM PMSF) for 2 h at 4°C. Protein-bound beads were washed with IP buffer for five times and then incubated with 1 μg MBP as a control or with 1 μg MBP-ABS6_C in IP buffer for 2 h at 4°C. Finally, beads were spun down, washed with IP buffer for five times, and boiled in 2× SDS sample buffer (125 mM Tris-HCl pH 6.8, 20% glycerol, 4% SDS, and 0.005% bromophenol blue) for 5 min. Elutes were analyzed by immunoblotting with anti-KTN1 and anti-MBP antibodies.

The GST pull-down assay was performed using the GST Protein Interaction Pull-Down Kit (21516, Pierce) with 10 μg GST-SAV4, 10 μg M-ABS6_C-H, and 20 μl glutathione agarose. Equal amounts of GST and MBP-His served as negative controls. After pull-down, elutes were analyzed by immunoblotting with anti-GST and anti-His antibodies.

EDTA-free cOmplete Protease Inhibitor Cocktail (04693132001, Roche) was added to a 1× final concentration in all buffers used for Co-IP and pull-down assays.

In vitro MT assays

In all *in vitro* MT assays, purified MBP-ABS6_C-His and MBP-His were first diafiltrated and concentrated with PEM buffer (80 mM PIPES pH 7.0, 2 mM $MgCl_2$, and 0.5 mM EGTA) using the concentrator devices (88513, Pierce), and centrifuged at 100,000 g for 15 min at 4°C to remove protein aggregates.

The MT co-sedimentation assay and polymerization assay were carried out using commercial kits (BK029 and BK006, Cytoskeleton, Inc.). To visualize MT bundling, rhodamine-labeled tubulin (TL590M, Cytoskeleton, Inc.) or label-free tubulin (TL238, Cytoskeleton, Inc.) were polymerized in PEM buffer with 1 mM GTP and 10% glycerol and stabilized with taxol following procedures described by the manufacturer. After polymerization, MTs were spun down at 100,000 g for 30 min at 37°C to remove the unpolymerized tubulins and resuspended in PEM buffer with 20 μM taxol. MTs were incubated with the indicated recombinant proteins for 10 min before examination. Rhodamine-labeled MTs were examined by a fluorescent microscope (DM5000B, Leica). Label-free MTs were negative stained and examined by a transmission electron microscope (HT7700, Hitachi) following a standard protocol (Moores 2008).

Co-IP

Co-IP was performed following procedures described in Avila et al. (2015). Briefly, membrane fractions were prepared from 7-day-old seedlings. Solubilized membranes were incubated with GFP-Trap agarose beads (gta-20, ChromoTek) in IP buffer (100 mM Tris-HCl pH 7.3, 150 mM NaCl, 1% Triton X-100, 1 mM EDTA, and 10% glycerol) overnight at 4°C. After IP, GFP-Trap beads were washed five times in wash buffer (10 mM Tris-HCl pH 7.3, 150 mM NaCl, and 0.5 mM EDTA) and boiled in 2× SDS sample buffer for 5 min. Immunoprecipitated proteins were analyzed by immunoblotting with anti-GFP and anti-KTN1 antibodies. EDTA-free cOmplete Protease Inhibitor Cocktail (04693132001, Roche) was added to a 1× final concentration in all buffers used during sample preparation and IP.

Antibodies

Polyclonal antibody against KTN1 was prepared in-house following the same design in Lin et al. (2013). Other antibodies used in this study are anti-GST (ab19256, Abcam), anti-His (ab18184, Abcam), anti-MBP (ab65, Abcam), and anti-GFP (632381, Clontech).

Drug treatment

1-aminocyclopropane-1-carboxylate (ACC) (A1178, TCI) was prepared as a 100 mM stock in deionized water. Oryzalin (36182, Sigma) was prepared as a 10 mM stock in DMSO. Taxol (TXD01, Cytoskeleton, Inc.) was prepared as a 2 mM stock in DMSO.

For hook angle analysis, 10 μM ACC was added to the 1/2 MS medium. 0.5 μM oryzalin, 1 μM taxol or equal volume of DMSO was added to the medium with or without 10 μM ACC. 3-day-old etiolated seedlings were photographed with a CCD camera (DS-Ri2, Nikon) mounted on a stereoscope (SMZ25, Nikon). Hook angles were measured with Fiji-ImageJ software.

To treat protoplasts with oryzalin, protoplasts were incubated in W5 solution (2 mM MES pH 5.7, 154 mM NaCl, 125 mM $CaCl_2$, and 5 mM KCl). for 12 h after transfection and then treated with 10 μM oryzalin for 1 h. After treatment, protoplasts were washed in W5 solution and examined with confocal microscopy.

Accession numbers

Sequence data used in this article can be found in NCBI databases under the following accession numbers: *ABS6*, At4G10640; *KTN1*, AT1G80350; *SAV4*, AT5G10200.

ACKNOWLEDGMENTS

We thank the Teaching and Research Core Facility at the College of Life Sciences, NWAFU for support in this work. This work was supported by grants from the National Natural Science Foundation of China (31770205 and 31970186 to X.L., 31870268 to F.Y.).

AUTHOR CONTRIBUTIONS

X.L. and F.Y. conceived and designed the study. Yuanfeng Li, M.D., H.L., Yan Li, H.X., Y.C., and J.Z. performed the experiments. Yuanfeng Li and M.J. analyzed

data. Y.Q., J.S., and L.A. provided technical assistance. X.L. and F.Y. wrote the manuscript. All authors discussed the results and commented on the manuscript.

REFERENCES

Abel S, Savchenko T, Levy M (2005) Genome-wide comparative analysis of the IQD gene families in *Arabidopsis thaliana* and *Oryza sativa*. **BMC Evol Biol** 5: 72

Ambrose C, Allard JF, Cytrynbaum EN, Wasteneys GO (2011) A CLASP-modulated cell edge barrier mechanism drives cell-wide cortical microtubule organization in *Arabidopsis*. **Nat Commun** 2: 430

Avila JR, Lee JS, Torii KU (2015) Co-immunoprecipitation of membrane-bound receptors. **Arabidopsis Book** 13: e0180

Baskin TI (2001) On the alignment of cellulose microfibrils by cortical microtubules: A review and a model. **Protoplasma** 215: 150**–**171

Bichet A, Desnos T, Turner S, Grandjean O, Hofte H (2001) BOTERO1 is required for normal orientation of cortical microtubules and anisotropic cell expansion in *Arabidopsis*. **Plant J** 25: 137–148

Boudaoud A, Burian A, Borowska-Wykret D, Uyttewaal M, Wrzalik R, Kwiatkowska D, Hamant O (2014) FibrilTool, an ImageJ plug-in to quantify fibrillar structures in raw microscopy images. **Nat Protoc** 9: 457–463

Bouquin T, Mattsson O, Naested H, Foster R, Mundy J (2003) The *Arabidopsis* lue1 mutant defines a katanin p60 ortholog involved in hormonal control of microtubule orientation during cell growth. **J Cell Sci** 116: 791–801

Burk DH, Liu B, Zhong R, Morrison WH, Ye ZH (2001) A katanin-like protein regulates normal cell wall biosynthesis and cell elongation. **Plant Cell** 13: 807–827

Bürstenbinder K, Moller B, Plotner R, Stamm G, Hause G, Mitra D, Abel S (2017) The IQD family of calmodulin-binding proteins links calcium signaling to microtubules, membrane subdomains, and the nucleus. **Plant Physiol** 173: 1692–1708

Bürstenbinder K, Savchenko T, Muller J, Adamson AW, Stamm G, Kwong R, Zipp BJ, Dinesh DC, Abel S (2013) *Arabidopsis* calmodulin-binding protein IQ67-domain 1 localizes to microtubules and interacts with kinesin light chain-related protein-1. **J Biol Chem** 288: 1871–1882

Chen X, Wu S, Liu Z, Friml J (2016) Environmental and endogenous control of cortical microtubule orientation. **Trends Cell Biol** 26: 409–419

Cheung K, Senese S, Kuang J, Bui N, Ongpipattanakul C, Gholkar A, Cohn W, Capri J, Whitelegge JP, Torres JZ (2016) Proteomic analysis of the mammalian katanin family of microtubule-severing enzymes defines katanin p80 subunit B-like 1 (KATNBL1) as a regulator of mammalian katanin microtubule-severing. **Mol Cell Proteomics** 15: 1658–1669

Clough SJ, Bent AF (1998) Floral dip: A simplified method for agrobacterium-mediated transformation of *Arabidopsis* thaliana. **Plant J** 16: 735–743

Deinum EE, Tindemans SH, Lindeboom JJ, Mulder BM (2017) How selective severing by katanin promotes order in the plant cortical microtubule array. **Proc Natl Acad Sci USA** 114: 6942–6947

Dixit R, Cyr, R (2004) Encounters between dynamic cortical microtubules promote ordering of the cortical array through angle-dependent modifications of microtubule behavior. **Plant Cell** 16: 3274–3284.

Ehrhardt DW, Shaw SL (2006) Microtubule dynamics and organization in the plant cortical array. **Annu Rev Plant Biol** 57: 859–875

Elliott A, Shaw SL (2018) Update: Plant Cortical Microtubule Arrays. **Plant Physiol** 176: 94–105

Fan Y, Burkart GM, Dixit R (2018) The *Arabidopsis* SPIRAL2 protein targets and stabilizes microtubule minus ends. **Curr Biol** 28: 987–994 e983

Fu Y, Xu T, Zhu L, Wen M, Yang Z (2009) A ROP GTPase signaling pathway controls cortical microtubule ordering and cell expansion in *Arabidopsis*. **Curr Biol** 19: 1827–1832

Ge Y, Yan F, Zourelidou M, Wang M, Ljung K, Fastner A, Hammes UZ, Di Donato M, Geisler M, Schwechheimer C, Tao Y (2017) SHADE AVOIDANCE 4 is required for proper auxin distribution in the hypocotyl. **Plant Physiol** 173: 788–800

Gutierrez R, Lindeboom JJ, Paredez AR, Emons AM, Ehrhardt DW (2009) *Arabidopsis* cortical microtubules position cellulose synthase delivery to the plasma membrane and interact with cellulose synthase trafficking compartments. **Nat Cell Biol** 11: 797–806

Guzman P, Ecker JR (1990) Exploiting the triple response of *Arabidopsis* to identify ethylene-related mutants. **Plant Cell** 2: 513–523

Hamada T (2014) Microtubule organization and microtubule-associated proteins in plant cells. **Int Rev Cell Mol Biol** 312: 1–52

Hartman JJ, Mahr J, McNally K, Okawa K, Iwamatsu A, Thomas S, Cheesman S, Heuser J, Vale RD, McNally FJ (1998) Katanin, a microtubule-severing protein, is a novel AAA ATPase that targets to the centrosome using a WD40-containing subunit. **Cell** 93: 277–287

Jia M, Liu X, Xue H, Wu Y, Shi L, Wang R, Chen Y, Xu N, Zhao J, Shao J, Qi Y, An L, Sheen J, Yu F (2019) Noncanonical ATG8-ABS3 interaction controls senescence in plants. **Nat Plants** 5: 212–224

Jiang K, Rezabkova L, Hua S, Liu Q, Capitani G, Altelaar AFM, Heck AJR, Kammerer RA, Steinmetz MO, Akhmanova A (2017) Microtubule minus-end regulation at spindle poles by an ASPM-katanin complex. **Nat Cell Biol** 19: 480–492

Kieber JJ, Rothenberg M, Roman G, Feldmann KA, Ecker JR (1993) CTR1, a negative regulator of the ethylene response pathway in *Arabidopsis*, encodes a member of the raf family of protein kinases. **Cell** 72: 427–441

Liang H, Zhang Y, Martinez P, Rasmussen CG, Xu T, Yang Z (2018) The microtubule-associated protein IQ67 DOMAIN5 modulates microtubule dynamics and pavement cell shape. **Plant Physiol** 177: 1555–1568

Lin D, Cao L, Zhou Z, Zhu L, Ehrhardt D, Yang Z, Fu Y (2013) Rho GTPase signaling activates microtubule severing to promote microtubule ordering in *Arabidopsis*. **Curr Biol** 23: 290–297

Lindeboom JJ, Nakamura M, Hibbel A, Shundyak K, Gutierrez R, Ketelaar T, Emons AM, Mulder BM, Kirik V, Ehrhardt DW (2013) A mechanism for reorientation of cortical microtubule arrays driven by microtubule severing. **Science** 342: 1245533

Lukowitz W, Gillmor CS, Scheible WR (2000) Positional cloning in *Arabidopsis*. Why it feels good to have a genome initiative working for you. **Plant Physiol** 123: 795–805

Luo D, Oppenheimer DG (1999) Genetic control of trichome branch number in *Arabidopsis*: the roles of the FURCA loci. **Development** 126: 5547–5557

Ma Q, Sun J, Mao T (2016) Microtubule bundling plays a role in ethylene-mediated cortical microtubule reorientation in etiolated *Arabidopsis* hypocotyls. **J Cell Sci** 129: 2043–2051

McNally FJ, Roll-Mecak A (2018) Microtubule-severing enzymes: From cellular functions to molecular mechanism. **J Cell Biol** 217: 4057–4069

McNally FJ, Thomas S (1998) Katanin is responsible for the M-phase microtubule-severing activity in Xenopus eggs. **Mol Biol Cell** 9: 1847–1861

McNally FJ, Vale RD (1993) Identification of katanin, an ATPase that severs and disassembles stable microtubules. **Cell** 75: 419–429

Mestek Boukhibar L, Barkoulas M (2016) The developmental genetics of biological robustness. **Ann Bot** 117: 699–707

Moores C (2008) Studying microtubules by electron microscopy. **Methods Cell Biol** 88: 299–317

Nakamura M (2015) Microtubule nucleating and severing enzymes for modifying microtubule array organization and cell morphogenesis in response to environmental cues. **New Phytol** 205: 1022–1027

Nakamura M, Ehrhardt DW, Hashimoto T (2010) Microtubule and katanin-dependent dynamics of microtubule nucleation complexes in the acentrosomal *Arabidopsis* cortical array. **Nat Cell Biol** 12: 1064–1070

Nakamura M, Naoi K, Shoji T, Hashimoto T (2004) Low concentrations of propyzamide and oryzalin alter microtubule dynamics in *Arabidopsis* epidermal cells. **Plant Cell Physiol** 45: 1330–1334

Paredez AR, Somerville CR, Ehrhardt DW (2006) Visualization of cellulose synthase demonstrates functional association with microtubules. **Science** 312: 1491–1495

Roll-Mecak A, Vale RD (2006) Making more microtubules by severing: a common theme of noncentrosomal microtubule arrays? **J Cell Biol** 175: 849–851

Sampathkumar A, Krupinski P, Wightman R, Milani P, Berquand A, Boudaoud A, Hamant O, Jonsson H, Meyerowitz EM (2014) Subcellular and supracellular mechanical stress prescribes cytoskeleton behavior in *Arabidopsis* cotyledon pavement cells. **Elife** 3: e01967

Schaefer E, Belcram K, Uyttewaal M, Duroc Y, Goussot M, Legland D, Laruelle E, de Tauzia-Moreau ML, Pastuglia M, Bouchez D (2017) The preprophase band of microtubules controls the robustness of division orientation in plants. **Science** 356: 186–189

Srayko M, Buster DW, Bazirgan OA, McNally FJ, Mains PE (2000) MEI-1/MEI-2 katanin-like microtubule severing activity is required for Caenorhabditis elegans meiosis. **Genes Dev** 14: 1072–1084

Stoppin-Mellet V, Gaillard J, Vantard M (2002) Functional evidence for *in vitro* microtubule severing by the plant katanin homologue. **Biochem J** 365: 337–342

Sugiyama Y, Wakazaki M, Toyooka K, Fukuda H, Oda Y (2017) A novel plasma membrane-anchored protein regulates xylem cell-wall deposition through microtubule-dependent lateral inhibition of Rho GTPase domains. **Curr Biol** 27: 2522-2528 e2524

Tian J, Kong Z (2019) The role of the augmin complex in establishing microtubule arrays. **J Exp Bot** 70: 3035–3041

Uyttewaal M, Burian A, Alim K, Landrein B, Borowska-Wykret D, Dedieu A, Peaucelle A, Ludynia M, Traas J, Boudaoud A, Kwiatkowska D, Hamant O (2012) Mechanical stress acts via katanin to amplify differences in growth rate between adjacent cells in *Arabidopsis*. **Cell** 149: 439–451

Vineyard L, Elliott A, Dhingra S, Lucas JR, Shaw SL (2013) Progressive transverse microtubule array organization in hormone-induced *Arabidopsis* hypocotyl cells. **Plant Cell** 25: 662–676

Waadt R, Schmidt LK, Lohse M, Hashimoto K, Bock R, Kudla J (2008) Multicolor bimolecular fluorescence complementation reveals simultaneous formation of alternative CBL/CIPK complexes in planta. **Plant J** 56: 505–516

Wang C, Liu W, Wang G, Li J, Dong L, Han L, Wang Q, Tian J, Yu Y, Gao C, Kong Z (2017) KTN80 confers precision to microtubule severing by specific targeting of katanin complexes in plant cells. **EMBO J** 36: 3435–3447

Wang G, Wang C, Liu W, Ma Y, Dong L, Tian J, Yu Y, Kong Z (2018) Augmin antagonizes katanin at microtubule crossovers to control the dynamic organization of plant cortical arrays. **Curr Biol** 28: 1311–1317 e1313

Wang R, Liu X, Liang S, Ge Q, Li Y, Shao J, Qi Y, An L, Yu F (2015) A subgroup of MATE transporter genes regulates hypocotyl cell elongation in *Arabidopsis*. **J Exp Bot** 66: 6327–6343

Wasteneys GO (2000) The cytoskeleton and growth polarity. **Curr Opin Plant Biol** 3: 503–511

Webb M, Jouannic S, Foreman J, Linstead P, Dolan L (2002) Cell specification in the *Arabidopsis* root epidermis requires the activity of ECTOPIC ROOT HAIR 3--a katanin-p60 protein. **Development** 129: 123–131

Weigel D, Ahn JH, Blazquez MA, Borevitz JO, Christensen SK, Fankhauser C, Ferrandiz C, Kardailsky I, Malancharuvil EJ, Neff MM, Nguyen JT, Sato S, Wang ZY, Xia Y, Dixon RA, Harrison MJ, Lamb CJ, Yanofsky MF, Chory J (2000) Activation tagging in *Arabidopsis*. **Plant Physiol** 122: 1003–1013

Wightman R, Chomicki G, Kumar M, Carr P, Turner SR (2013) SPIRAL2 determines plant microtubule organization by modulating microtubule severing. **Curr Biol** 23: 1902–1907

Wightman R, Turner SR (2007) Severing at sites of microtubule crossover contributes to microtubule alignment in cortical arrays. **Plant J** 52: 742–751

Xiang C, Han P, Lutziger I, Wang K, Oliver DJ (1999) A mini binary vector series for plant transformation. **Plant Mol Biol** 40: 711–717

Xiao H, Jiang N, Schaffner E, Stockinger EJ, van der Knaap E (2008) A retrotransposon-mediated gene duplication underlies morphological variation of tomato fruit. **Science** 319: 1527–1530

Yoo SD, Cho YH, Sheen J (2007) *Arabidopsis* mesophyll protoplasts: A versatile cell system for transient gene expression analysis. **Nat Protoc** 2: 1565–1572

Yu F, Park S, Rodermel SR (2004) The *Arabidopsis* FtsH metalloprotease gene family: Interchangeability of subunits in chloroplast oligomeric complexes. **Plant J** 37: 864–876

Zehr E, Szyk A, Piszczek G, Szczesna E, Zuo X, Roll-Mecak A (2017) Katanin spiral and ring structures shed light on power stroke for microtubule severing. **Nat Struct Mol Biol** 24: 717–725

Zhang Q, Fishel E, Bertroche T, Dixit R (2013) Microtubule severing at crossover sites by katanin generates ordered cortical microtubule arrays in *Arabidopsis*. **Curr Biol** 23: 2191–2195

Figures

Figure 1. ABS6 promotes cMT ordering and directly binds MTs

(**A**) Transverse cMT arrays underpin anisotropic plant cell elongation. (**B**) Seedling morphology, cotyledon abaxial PCs, and PC cMT arrays of 7-day-old wild type (WT) and *abs6-1D* seedlings. Bars: 2 mm for seedlings, 50 μm for PCs, 10 μm for cMTs. (**C**) Heatmap showing the frequency distribution of cMT angles in cotyledon abaxial PCs of 7-day-old WT and *abs6-1D* seedlings. Angles of individual cMTs were measured (WT, n = 1076 cMTs in 15 cells; *abs6-1D*, n = 1007 cMTs in 18 cells). (**D)** Confocal imaging of cMTs and ABS6-GFP in cotyledon abaxial PCs of a 7-day-old *p35S:mRFP-TUB6 p35S:ABS6-GFP* dual-labeled line. Bar: 10 μm. (**E)** ABS6-GFP and mRFP-TUB6 signal intensities along the white line indicated in (**D**). a.u., arbitrary units. (**F**) *ABS6* gene model. Exons and introns are represented by boxes and lines, respectively. 5′- and 3′-untranslated regions are shaded in grey. (**G**) Transient expression of *p35S:ABS6-GFP*, *p35S:ABS6_N-GFP*, or *p35S:ABS6_C-GFP* in protoplasts from the *mRFP-TUB6* line. Bar: 10 μm. (**H**) M-ABS6_C-H (a recombinant ABS6_C with a N-terminal MBP tag and a C-terminal His tag) binds MTs in the MT co-sedimentation assay. MBP-His served as a negative control.

Figure 1

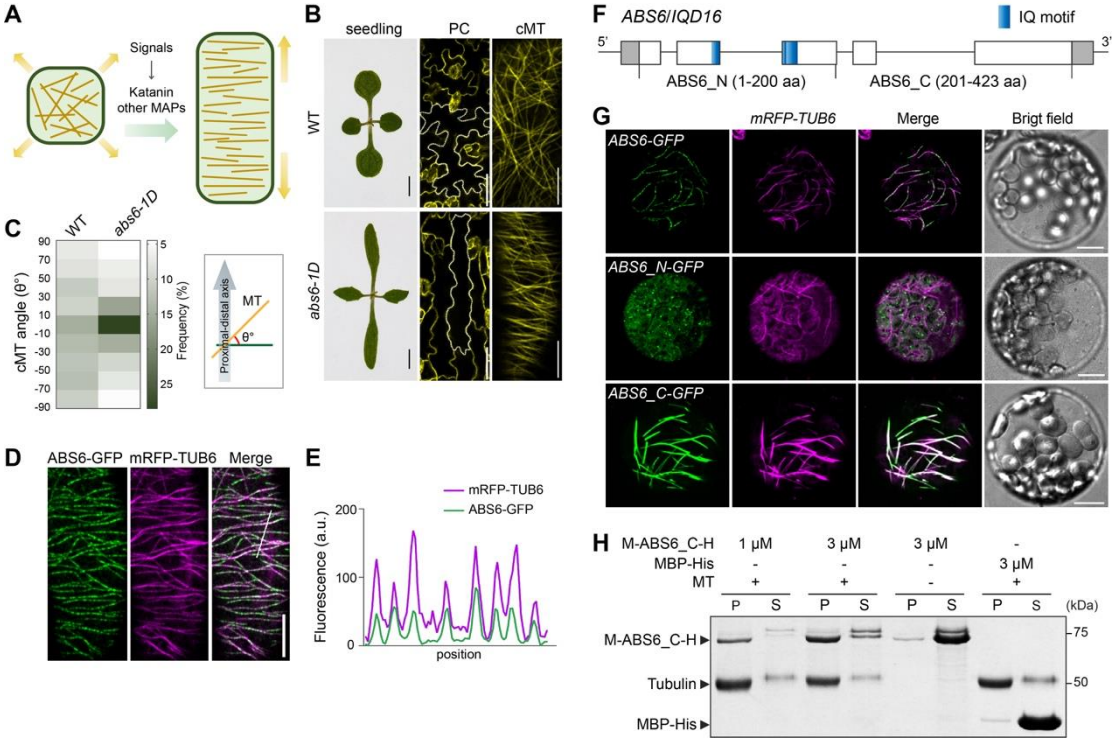

Figure 2. MT stabilization and bundling effects of ABS6_C

(**A**) ABS6_C-GFP bundles and stabilizes cMTs in protoplasts. Protoplasts from the *mRFP-TUB6* line transiently expressing ABS6_C-GFP or ABS6-GFP were treated with oryzalin or mock treated with an equal amount of DMSO for 1 hr before confocal imaging. Images of the RFP channel are also shown in "Fire" spectrum using ImageJ to highlight the differences in mRFP-TUB6 fluorescence intensity. Bars: 10 μm. (**B**) Effects of ABS6_C on tubulin polymerization *in vitro*. A standard tubulin polymerization reaction was carried out in the presence of 1 mM GTP and 10% glycerol in PEM buffer. Tubulin polymerization was determined by measuring the absorbance at 340 nm. Shown are polymerization reactions containing 0.3 μM M-ABS6_C-H, 0.5 μM M-ABS6_C-H, 0.5 μM MBP-His, or 10 μM taxol compared to the control reaction. (**C**) Effects of ABS6_C on MT bundling *in vitro*. Taxol-stabilized MTs were incubated with MBP-His, M-ABS6_C-H, or PEM buffer alone and examined with fluorescence microcopy (FM) and transmission electron microscopy (TEM). For the salt treatment, 0.2 M NaCl was added to the mixture after incubating MTs with M-ABS6_C-H for 10 min. Rhodamine-labeled

tubulin was used for FM. Label-free tubulin was used for TEM. Bars: 10 μm for FM, 200 nm for TEM.

Figure 2

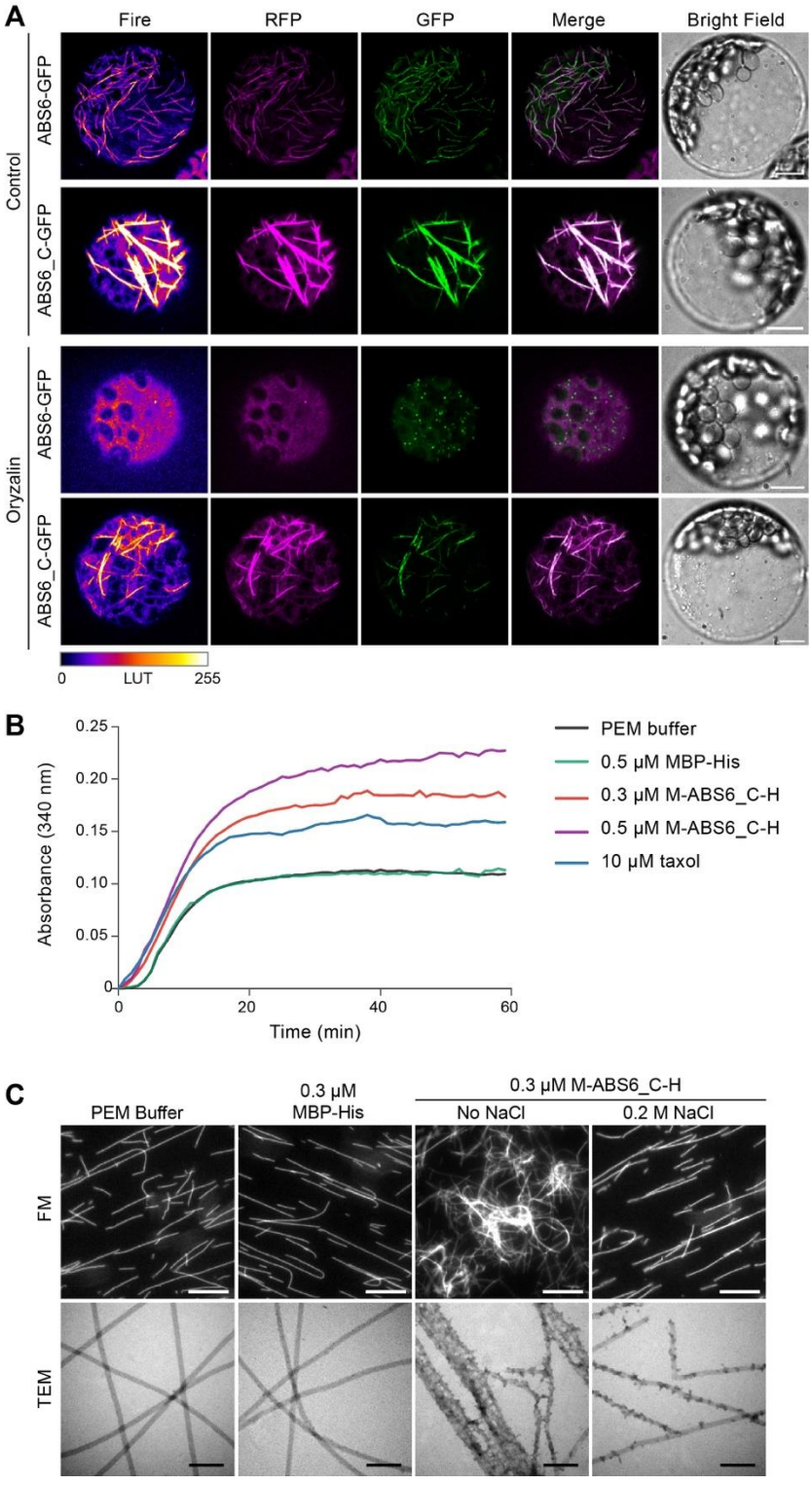

Figure 3. ABS6-mediated cMT ordering requires KTN1 and SAV4

(**A**) and (**B**) Mutant alleles of *ktn1* (**A**) and *sav4* (**B**) identified in our *abs6-1D* suppressor screen. Gene models are shown as in Figure 1F. (**C**) Seedlings, cotyledon abaxial PCs, and PC cMT arrays in 7-day-old seedlings of the indicated genotypes. Bars: 2 mm for seedlings, 50 μm for PCs, 10 μm for cMTs. (**D**) and (**E**) Quantification of the leaf index (**D**) and PC length (**E**) in the genotypes shown in (**C**). Data are means ± standard deviation (*SD*) (n=10). **, $p<0.01$; ****, $p<0.0001$, unpaired t-test. (**F**) Heatmap showing the frequency distribution of cMT angles in cotyledon abaxial PCs of the indicated genotypes. cMT angles were measured as in Figure 1C. More than 1000 cMTs were analyzed for each genotype.

Figure 3

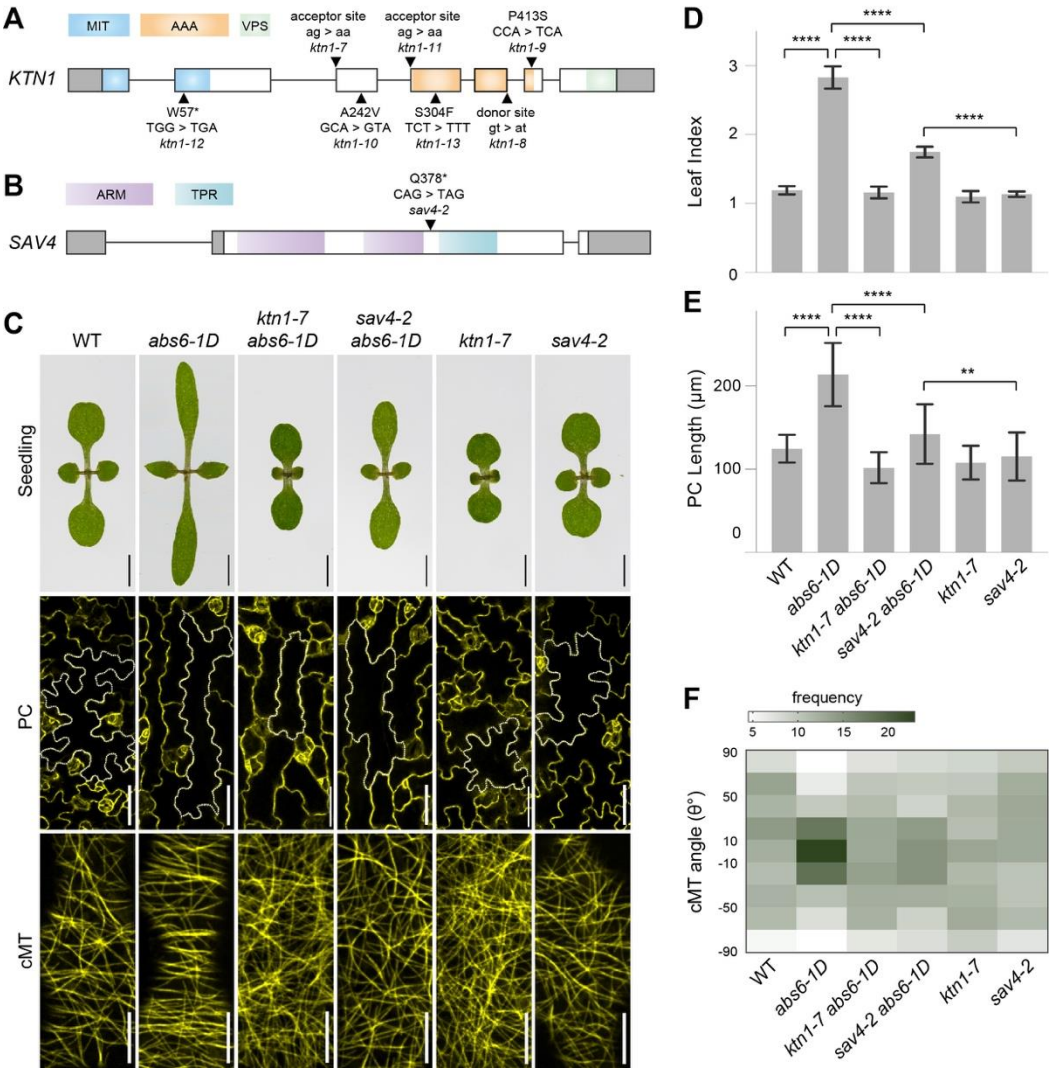

Figure 4. ABS6 and SAV4 are positive regulators of cMT severing.

(**A–C**) Dot plots (median with interquartile range, IQR) of cMT severing frequencies (**A**), severing waiting time (**B**), and severing probability (**C**) in cotyledon abaxial PCs of the indicated genotypes. Each symbol represents a randomly selected ROI used to score severing events (**A**), or a severing event (**B**), or a crossing over event (**C**). n.s., not significant; ****, p<0.0001, two-tailed Mann-Whitney test. (**D**) Cotyledon abaxial PCs of 4-day-old seedlings of *pKTN1:GFP-KTN1 p35S:mRFP-TUB6* dual-labeled lines in WT, *abs6-1D*, and *sav4-2* backgrounds were examined by confocal imaging. Bars: 5 µm. (**E**) Dot plots (median with IQR) of the proportion of cMT crossovers with GFP-KTN1 puncta in WT, *abs6-1D*, and *sav4-2* cells. Each symbol represents a randomly selected ROI used to score crossovers. ****, p<0.0001, two-tailed Mann-Whitney test.

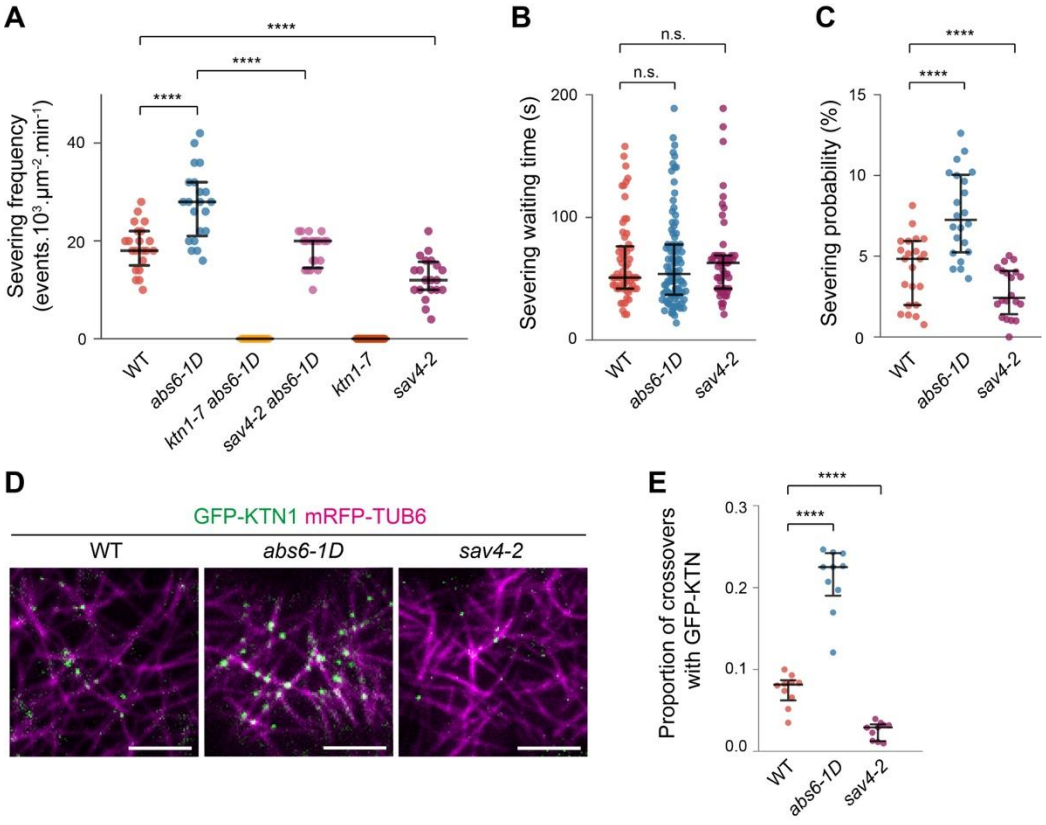

Figure 5. ABS6 promotes severing via direct interaction with KTN1

(**A**) Interaction of ABS6_C and KTN1 in the yeast two-hybrid assay. (**B**) *In vitro* Co-IP assay of MBP-ABS6_C and His-KTN1. MBP-ABS6_C or MBP were

incubated with His-KTN1, immunoprecipitated with anti-KTN1 antibody-conjugated Protein A beads and analyzed by immunoblotting with anti-KTN1 and anti-MBP antibodies. (**C**) Co-expression of *p35S:YN-ABS6_C* and *p35S:KTN1-YC* in protoplasts from the *mRFP-TUB6* line in the WT background. Bar: 10 μm. (**D**) Co-expression of *p35S:YN-ABS6* and *p35S:KTN1*^{R402A}*-YC* in protoplasts from the *mRFP-TUB6* line in the *ktn1-7* background. Bar: 10 μm. (**E**) Co-IP of KTN1 with ABS6-GFP. Membrane fractions isolated from 7-day-old *p35S:ABS6-GFP* lines in the WT or *ktn1-7* background were immunoprecipitated with GFP-Trap beads and analyzed by immunoblotting with anti-GFP and anti-KTN1 antibodies.

Figure 5

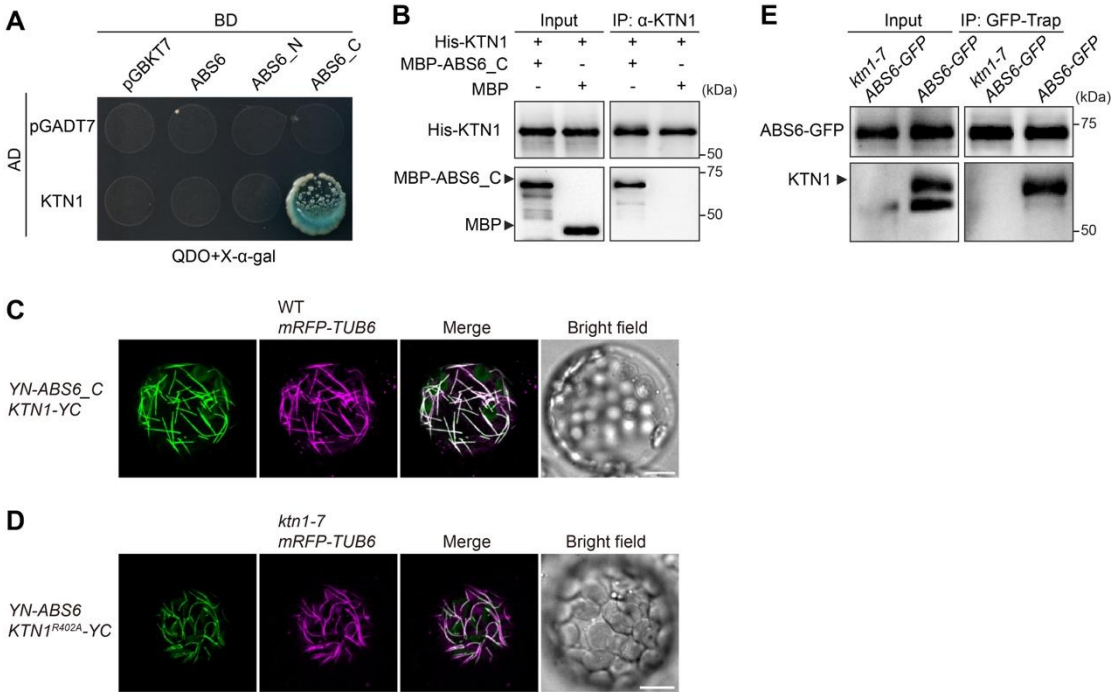

Figure 6. ABS6 interacts with SAV4 via its C-terminal half.

(**A**) Interaction of ABS6_C and SAV4 in the yeast two-hybrid assay. (**B**) *In vitro* pull-down of M-ABS6_C-H by GST-SAV4. MBP-His and GST served as negative controls. GST-SAV4 or GST were detected with an anti-GST antibody. M-ABS6_C-H or MBP-His were detected by an anti-MBP antibody. (**C**) Co-expression of *p35S:YN-SAV4* and *p35S:ABS6_C-YC* in protoplasts from the

mRFP-TUB6 line. Bars: 10 μm. (**D**) Cotyledon abaxial PCs of 4-day-old seedlings of *pSAV4:SAV4-GFP p35S:mRFP-TUB6* dual-labeled lines in the WT or *abs6-1D* background were examined by confocal imaging. Bars: 5 μm. (**E**) Dot plots (median with IQR) of the proportion of SAV4-GFP puncta localized to the cMTs. Each symbol represents a randomly selected ROI used to score SAV-GFP localization. n = 20, ***, $p < 0.001$, two-tailed Mann-Whitney test.

Figure 6

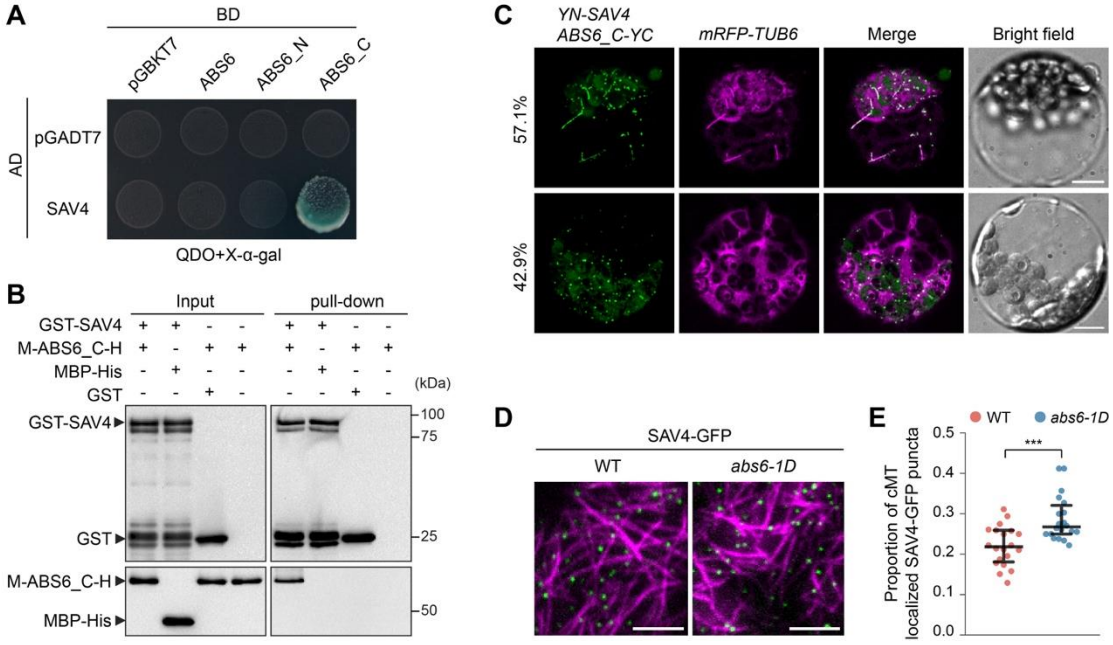

Figure 7. ABS6, SAV4, and KTN1 regulate the ethylene response in the apical hook

(**A**) Effects of MT drugs on apical hook formation. Shown are representative images of 3-day-old WT and *ctr1-1* seedlings grown in the dark on regular medium supplemented with 0.5 μM oryzalin, 1 μm taxol, or DMSO as a mock treatment. For "WT+ACC", 10 μM ACC was added to the medium in addition to the mock, oryzalin, or taxol treatment. Bars: 500 μm. (**B**) Dot plots (median with IQR) of hook angles of seedlings under the treatments shown in (**A**). (**C**) Effects of ACC on apical hook exaggeration in the indicated genotypes. Seedlings of the indicated genotypes were grown on regular medium (mock) or medium containing 10 μM ACC for 3 days in the dark prior to imaging. Bars: 500 μm. (**D**) Dot plots (median

with IQR) of hook angles of the indicated genotypes under mock or ACC treatment in (**C**). In dot plots (**B**) and (**D**), each symbol represents a hook angle measurement of one seedling. n > 120, ****, $p < 0.0001$, two-tailed Mann-Whitney test. (**E**) A working model for the regulation of cMT severing by ABS6 through its interactions with KTN1 and SAV4.

Figure 7